Optimization analysis on collection efficiency of vacuum cleaner based on two-fluid and CFD-DEM model

Lian Wang and Xihua Chu*

School of Civil Engineering, Wuhan University, Wuhan, 430072, Hubei, China

Abstract.   The reasonable layout of vacuum cleaner can effectively improve the collection efficiency of iron filings generated in the process of steel production. Therefore, in this study, the CFD-DEM coupling model and two-fluid model are used to calculate the iron filings collection efficiency of vacuum cleaner with different inclination/cross-sectional area, pressure drop and inlet angle. The results are as follows: The CFD-DEM coupling method can truly reflect the motion mode of iron filings in pneumatic conveying. Considering the instability and the decline of the growth rate of iron filings collection efficiency caused by high pressure drop, the layout of 75° inclination is suggested, and the optimal pressure drop is 100Pa. The optimal simulation results based on two-fluid model show that when the inlet angle and pressure drop are in the range of 45°~65° and 70Pa~100Pa, larger mass flow rate of iron filings can be obtained. It is hoped that the simulation results can offer some suggestion to the layout of vacuum cleaner in the rolling mill.

Keywords: CFD-DEM; iron filings collection efficiency; optimization analysis; two-fluid model; mass flow rate

1. Introduction

Plenty of ubiquitous iron filings generated in steel processing plants will not only endanger human health but also cause environmental pollution. As the collection equipment commonly used in steel processing plants is vacuum cleaner, it is of great significance to study the influence of the layout parameters of vacuum cleaner on the iron filings collection efficiency. The collection process of iron filings involves the movement of gas-solid two-phase flow, and the commonly simulation method for the gas-solid two-phase flow are based on Computational Fluid Dynamics and Discrete Element Method (CFD-DEM) coupling model or two-fluid model.

As for two-fluid model, both phases are treated as the continuum. The governing equations for solid phase and gas phase are locally averaged and similar. The gas is assumed to be incompressible. The particles are assumed to be spherical, frictionless, cohesionless and mono-dispersed. The detailed introduction and theory can refer to Patro's study (2014) in which the granular particles are described by the kinetic theory (Mathiesen *et al.* 2000, Ray *et al.* 2019, Patro and Dash 2014). Wherein Du (2006) investigated the impact of gas-solid drag models, the

---

*Corresponding author, Professor, E-mail: chuxh@whu.edu.cn

maximum packing limit and the restitution coefficient on the simulation of spouted fluidized beds based on two-fluid model.

Different from the two-fluid model, CFD-DEM coupling method can not only get a reasonable solution but also reflect the motion pattern of solid phase obviously as the motion of particles is calculated by Newton's laws as a discrete phase. And this approach has been recognized as an effective method to study the particle-fluid flow (Yu and Xu 2003, Zhu *et al*. 2007, Hobbs 2009). Since the discrete element method, a numerical simulation method for discontinuous media, was proposed by Cundall (1979), the CFD-DEM coupling method has gradually aroused the attention of researchers. For instance, Xu (2018) investigated the sedimentation process of non-cohesive particles by CFD-DEM method. Almohammed (2014) studied the influence of the gas flow rate on hydrodynamics of gas-solid flows in a three-dimensional, lab-scale spouted fluidized bed by Euler-Euler and Euler-Lagrange/DEM models. And the hydrodynamic behavior of the dense gas-solid flow in a laboratory scale spouted-fluid bed was investigated by Alobaid (2013) employing an in-house CFD/DEM code, which the fluid-particle interaction was determined with a new procedure called the offset method.

There are some reports in the research of pneumatic conveying in practical application (Miao *et al*. 2019; Dhurandhar *et al*. 2019; Zhang *et al*. 2018). Besides, Chu (2009) presented a mathematical model to describe the flow pattern of multiphase flow in dense medium cyclones by means of combining the Discrete Element Method with Computational Fluid Dynamics. Also, DPM model was used to optimize the structural parameters of electrostatic precipitator (Liu *et al*. 2018) and flexible membrane high temperature dust filter (Ma *et al*. 2019), which show that the addition of the guide plate and other components can significantly reduce the air flow heterogeneity in the chamber of the precipitator and improve its working stability. But there is no relevant report on the study of the collection efficiency of iron filings in rolling mill, therefore, in this paper, the CFD-DEM coupling method and two-fluid model are selected to optimize the iron filings collection efficiency with different specifications of simplified vacuum cleaner. And we hope to provide some reference for the layout of vacuum cleaner through the comparative analysis of the results.

2. Simulation methodology

2.1 CFD-DEM governing equations

The governing equations of the two phases refer to the Set II summarized by Zhou *et al*. (2010). The governing equations of the fluids based on the local mean variables in a computational cell are given respectively as:

$$\frac{\partial\left(\rho_f\varepsilon_f\right)}{\partial t}+\nabla\cdot\left(\rho_f\varepsilon_f\vec{u}_f\right)=0 \tag{1}$$

$$\frac{\partial\left(\rho_f\varepsilon_f\vec{u}_f\right)}{\partial t}+\nabla\cdot\left(\rho_f\varepsilon_f\vec{u}_f\vec{u}_f\right)=-\varepsilon_f\nabla p-\vec{F}_{p-f}+\nabla\cdot\left(\varepsilon_f\tau\right)+\rho_f\varepsilon_f\vec{g} \tag{2}$$

where ρ_f, ε_f, $\vec{u}_f$, p, τ and $\vec{F}_{p-f}$ are the fluid density, fluid volume fraction, fluid velocity, pressure, fluid viscous stress tensor and the volumetric particle-fluid interaction force, respectively. Among

them, the fluid volume fraction in a computational cell can be estimated through the equation of Hoomans *et al*. (1996):

$$\varepsilon_f = 1 - \frac{1}{V_{cell}} \sum_{i=1}^{k_v} \varphi_i V_i \qquad (3)$$

where k_v is the number of particles partially located within the fluid cell and $\varphi_i \in [0.1]$ denotes the volume fraction of particle i that belongs to the fluid cell as estimated through geometrical techniques. And the volumetric particle-fluid force and the fluid viscous stress tensor has the following form:

$$\vec{F}_{p-f} = \frac{1}{\Delta V} \sum_{i=1}^{n} \left(\vec{f}_{d,i} + \vec{f}_{vm,i} + \vec{f}_{B,i} + \vec{f}_{Saff,i} + \vec{f}_{Mag,i} \right) \qquad (4)$$

$$\tau = \mu \left[\left(\nabla \vec{u} + \nabla \vec{u}^T \right) - \frac{2}{3} \nabla \cdot \vec{u} I \right] \qquad (5)$$

where μ is the viscosity, I is the unit tensor, and $\vec{f}_d$, $\vec{f}_{vm}$, $\vec{f}_B$, $\vec{f}_{Saff}$ and $\vec{f}_{Mag}$ are the drag force, virtual mass force, Basset force, Saffman force and Magnus force, respectively. Conversely, the particle flow is treated as a discrete phase described by DEM. The equations of motion for individual spherical particle i with the mass m_i and the moment of inertia I_i can be written as Zhou *et al*. (2010):

$$m_i \frac{d\vec{v}_i}{dt} = \vec{f}_i^{f-p} + \sum_{j=1}^{k_c} \left(\vec{f}_{ij}^c + \vec{f}_{ij}^{nc} \right) + \vec{f}_i^g \qquad (6)$$

$$I_i \frac{d\vec{\omega}_i}{dt} = \sum_{j=1}^{k_c} \left(\vec{M}_{ij}^c + \vec{M}_i^{f-p} \right) \qquad (7)$$

where $\vec{v}_i$ and $\vec{\omega}_i$ are the translational and angular velocities of particle i, respectively. $\vec{f}_{ij}^c$ and $\vec{M}_{ij}^c$ are the contact force and torque (tangential and rolling torques) acting on particle i by particle j or wall. k_c is the number of particles or wall in interaction with the particle i and $\vec{f}_i^g = m_i \vec{g}$ is the gravitational body force. The interaction force between fluid and particle is $\vec{f}_i^{f-p}$. Also, $\vec{M}_i^{f-p}$ is known as fluid rotational resistance torque.

The particle-fluid interaction forces acting on individual particles can be written as (Crowe, Sommerfeld & Tsuji 1998):

$$\vec{f}_i^{f-p} = \vec{f}_{d,i} + \vec{f}_{\nabla p,i} + \vec{f}_{\nabla \cdot \tau,i} + \vec{f}_{vm,i} + \vec{f}_{B,i} + \vec{f}_{Saff,i} + \vec{f}_{Mag,i} \qquad (8)$$

where $\vec{f}_{\nabla p}$ represents the pressure gradient force which includes buoyancy force and $\vec{f}_{\nabla \tau}$ represents the viscous force. As for Ergun and Wen and Yu drag model (Gidaspow 1994) which is appropriate for dilute or dense systems, the drag force can be described as:
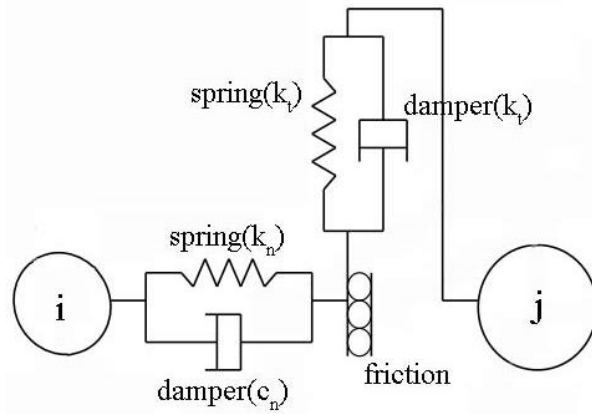
Fig. 1 Hertz-Mindlin contact model

$$\vec{f}_{drag} = \begin{cases} \dfrac{75\pi\mu_f d_p(1-\varepsilon_f)}{3\varepsilon_f}(\vec{u}_f - \vec{u}_p) + \dfrac{1.75\pi\mu_f d_p}{6\varepsilon_f}Re_p(\vec{u}_f - \vec{u}_p)\varepsilon_f \le 0.8 \\ \qquad\dfrac{C_D\pi\mu_f d_p}{8\varepsilon_f^{2.65}}Re_P(\vec{u}_f - \vec{u}_p) \qquad \varepsilon_f > 0.8 \end{cases} \tag{9}$$

here C_D is calculated based on the following equation:

$$C_D = \begin{cases} \dfrac{24}{Re_p}\left(1 + 0.15Re_p^{0.687}\right) & Re_p \le 1000 \\ 0.44 & Re_p > 1000 \end{cases} \tag{10}$$

The symbol Re_p stands for the particles Reynolds number defined as:

$$Re_p = \frac{\rho_f \varepsilon_f d_p}{\mu_f}\left|\vec{u}_f - \vec{u}_p\right| \tag{11}$$

The coupling between the fluid and particle is numerically achieved as follows. At each time step, the DEM provides information such as the positions and velocities of particles for the evaluation of volume fraction and particle-fluid interaction force in each computational cell. The CFD model then use the results to determine the flow field. Based on flow information such as fluid velocity and pressure distribution, the particle-fluid interaction forces can be converged. Incorporating the result forces into the DEM can determine the motion of individual particles in the next time step (Xu and Yu 1997). The contact model between particles in discrete element method is shown as Fig. 1.

2.2 Design exploration

Design exploration is a powerful approach for designing and understanding the analysis of parts and assemblies. It uses a deterministic method based on design of experiments (DOE) and

various optimization methods, with parameters as its fundamental components and describes the relationship between the design variables and the performance of the product, combined with response surfaces. The main purpose of design exploration is to identify the relationship between the performance of the product and the design variables. Design of experiments is a technique used to determine the location of sampling points and is included as part of the response surface, goal driven optimization and six sigma analysis systems. The design of experiments tab allows you to preview or generate and solve a DOE design point matrix. On the DOE tab, it can set the input parameter limits, set the properties of the DOE solve, view the table of design points and view several parameter charts (DesignXplorer 2013).

Optimization analysis module embedded in ANSYS program based on the sensitivity of the objective function to the design variables, providing a series of analytical-evaluation-correction cycle processes. Analyze the initial design, evaluate the analysis results according to the design requirements, and then revise the design, this cycle process is repeated until all design requirements are met.

3. CFD-DEM coupling simulation

3.1 Geometry and simulation setup

Refer to the layout of each process in the steel processing plants, as shown in Fig. 2, Simplified model, as shown in Fig. 3, is established based on the shedding state of iron filings.

The red region in the Fig. 3(a) is the area (0.8m×0.5m) where iron filings are generated. The central coordinates are (0.7m, 0.75m, and 1.5m). According to the moving direction of the steel during the unwinding process, the angle between the plane and the positive Y axis is set to 15°. And when the simulation begins, the iron filings are generated at the speed of the 0~2m/s with arbitrary orientation in the region. The computational domain was meshed by tetrahedrons, as shown in Fig. 3(b), and the Eulerian coupling model is adopted as the local solid volume fraction exceeds 10%. The information of the grid and calculation parameters are shown in Table 1.
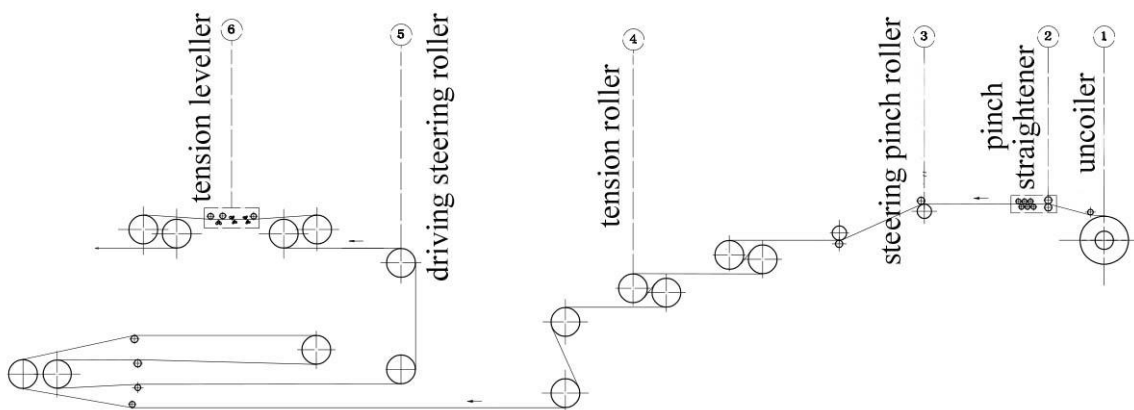

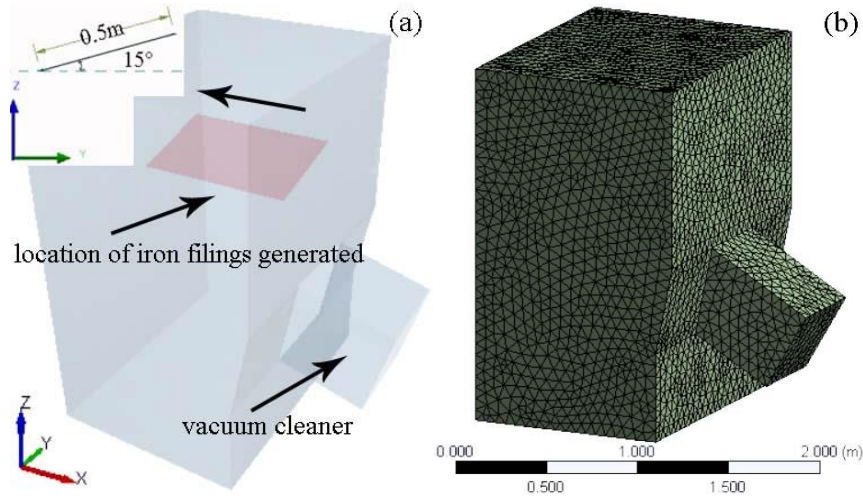Fig. 2 Procedure diagram of steel processing

Fig. 3 Simplified model for coupling calculation

Table 1 Grid information and calculation parameters

Nodes	13331
Elements	67236
Faces	138548
Minimum orthogonal quality	0.292
Standard deviation	0.095
Average skewness	0.23
Minimum volume(m^3)	5.2e^{-6}
Computational scale(m^3)	1.6×1.5×2
Turbulence model	Realizable κ–ε
Incline range(°)	30~120
Scope of the pressure drop (Pa)	40~140
Drag model	Ergun and Wen & Yu
Time step size(s)	0.002
Number of time steps	3000

The simulation of engineering problems involves a large number of particles and a large size of calculation domain, so the equivalent scaling method was usually adopted in order to reduce the time cost (Feng and Owen 2014). The real size of iron filings is about r=0.5mm, but for the convenience of calculation, the size is enlarged to r=6mm under the premise of acceptable similarity ratio. At the same time, in order to reflect the irregularity of iron filings, three spherical particles are nested each other to represent it. The calculation parameters are shown in Table 2.

3.2 Results and discussion

In this part, 42 sets of numerical calculations were carried out for analysis of the iron filings collection efficiency of the vacuum cleaner with different inclination (the angle between the vacuum cleaner and the negative Z axis is θ=30°, 45°, 60°, 75°, 90°, 105° and 120°, respectively)

Table 2 Summary of DEM parameters

|	
Iron filings radius (mm)	6
Iron filings equivalent density(kg/m3)	4.54
Poisson's ratio	0.28
Shear modulus(Pa)	7.7×10^6
Iron filings volume per combination(m^3)	1.88×10^{-6}
Iron filings mass per combination(kg)	8.55×10^{-6}
Initial velocity of iron filings(m/s)	0~2
Coefficient of restitution	0.45
Coefficient of static friction	0.55
Coefficient of rolling friction	0.3
Interaction model	Hertz-Mindlin
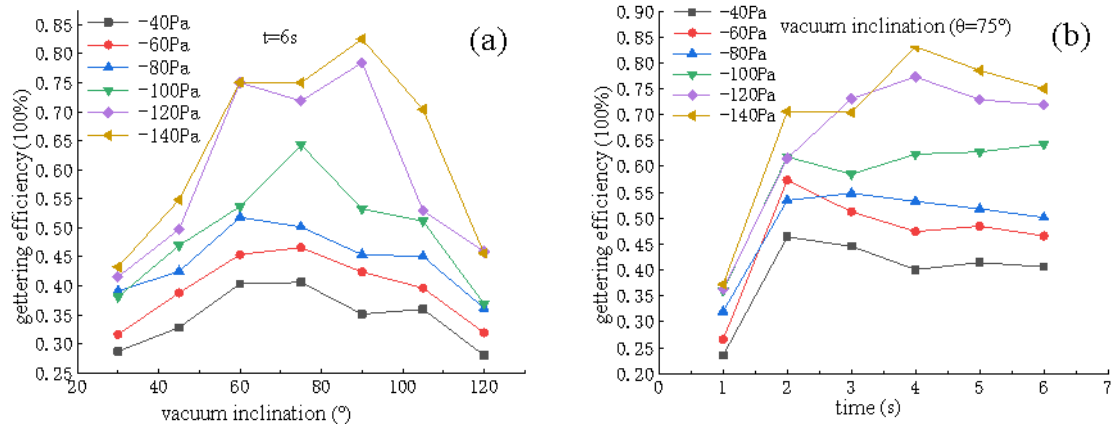
Fig. 4 The trend of collection efficiency with different parameters

and pressure drop (the outlet of the vacuum cleaner is negative pressure, and the other boundary is free atmospheric except the wall, i.e. ΔP=40Pa, 60Pa, 80Pa, 100Pa, 120Pa, 140Pa). It is noted that the change of inclination is corresponding to different cross-sectional areas as the inlet section area is fixed.

3.2.1 Iron filings collection efficiency

CFD-DEM coupling method is based on momentum exchange in each discretized fluid cell, with particle-induced force on fluid flow treated as a body force (Almohammed *et al*. 2014), and coupling calculation is dominated by the fluid phase. In this study, the time step is set as Δt = 0.002 *s* and the total time is 6s. The collection efficiency under different conditions is obtained by statistics of mass flow rate of the collection iron filings, as shown in Fig. 4.

As we can see from Fig. 4(a), the collection efficiency of iron filings varies from different conditions, with an average of about 48%. With the increase of the inclination of the vacuum cleaner, the iron filings collection efficiency in each pressure drop shows the overall trend of increasing first and then decreasing, and at the inclination of 30° and 120°, the collection efficiency is the minimum under the corresponding pressure drop. It is demonstrated that the collection efficiency can reach a satisfactory level when the inclination range of the vacuum

Table 3 Comparison of collection efficiency growth rate at 75° and 90°

pressure drop(Pa)	collection efficiency under 75° β (%)	growth rate η (%)	collection efficiency under 90° β (%)	growth rate η (%)
40	40.6	-	35.11	-
60	46.6	14.75	42.39	20.74
80	50.13	7.59	45.38	7.06
100	64.29	28.25	53.24	17.34
120	71.87	11.80	78.44	47.32
140	75.02	4.39	82.53	5.21

*notation: $\eta = (\beta_i - \beta_{i-1}) \cdot 100\% / \beta_{i-1}$

cleaner is 60° ~ 105°. Comparing the collection efficiency of each pressure drop in the inclination rang of 60° ~ 105°, it can be found that when the pressure drop is 40 Pa, 60 Pa and 100 Pa, the maximum collection efficiency occurs at 75°; the pressure drop changes to 120 Pa or 140 Pa, the maximum collection efficiency occurs at 90° and only when the pressure drop is 80Pa, can collection efficiency under 75° inclination reach the maximum. Therefore, it is ideal to lay the vacuum cleaner at the inclination of 75° or 90°. Next, we discuss the reasonable range of pressure drop at two inclinations. Table 3 shows the growth rate of iron filings collection efficiency with increasing pressure drop at inclination of 75° and 90°, It can be seen from the Table 3, when the pressure drops is 100Pa under the 75° inclination, the growth rate of collection efficiency is the largest, and when the pressure drops turn to 120Pa under the 90° inclination, the growth rate is the largest. According to the collection efficiency under different pressure drop, if the vacuum cleaner cannot provide enough pressure drop, the layout of 75° inclination should be selected, and the pressure drop can be set below 100 Pa. If the vacuum cleaner has enough power, it can be laid horizontally, and the pressure drop should be set at about 120 Pa. However, it should be noted that at both inclinations, when the growth rate of collection efficiency reaches its peak, it will decrease sharply with the increase of pressure drop. That is to say, if the pressure drop is increased equally at this time, the benefit will begin to decline.

Fig. 4(b) shows the curve of collection efficiency with time at different pressure drop when the inclination of vacuum cleaner is 75°. It can be seen from the figure that the coupling calculation process tends to be stable after 4s, especially under the condition of lower pressure drop, that is to say, with the increase of pressure drop, the calculation will become unstable, and this change is mainly manifested in the decreasing of collection efficiency, such as the result of 120Pa and 140Pa pressure drop. However, when the pressure drop is 100Pa, the collection efficiency changes steadily with time and shows an increasing trend, which is undoubtedly the most desirable for practical engineering. Therefore, it is suggested that the vacuum cleaner should be laid at 75° inclination, at which the optimal pressure drops is 100Pa, and the following content is based on that layout.

3.2.2 Physical parameter

By using the CFD-DEM coupling approach, not only the detailed results can be obtained, but also the interaction between the fluid and the solid phase, the motion pattern of the solid and the change of the mechanical parameters can be studied. The following analysis focus on the calculation results in each pressure drop when the inclination of the vacuum cleaner is 75°, and the flow field is shown in Fig. 5.
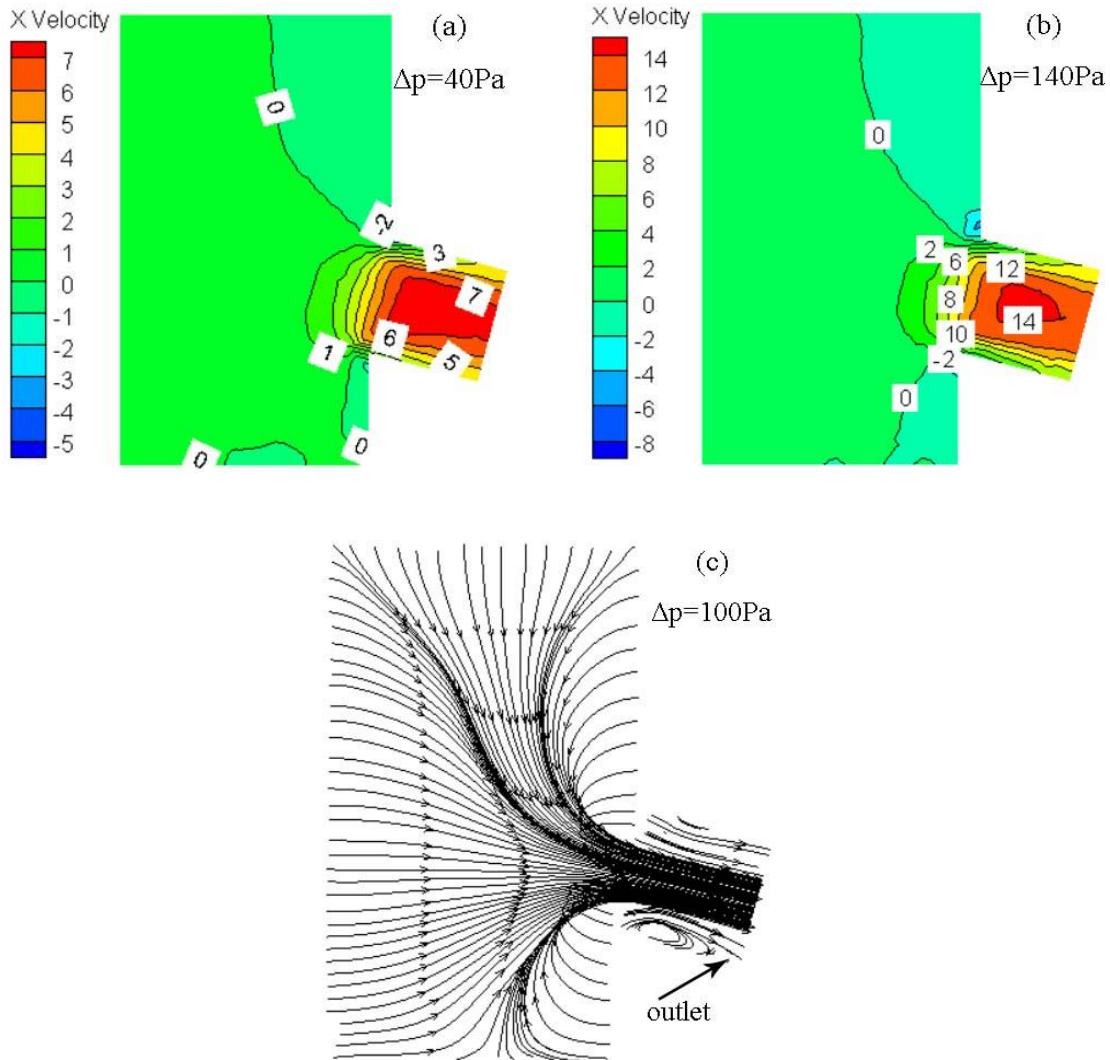
Fig. 5 Flow field and streamline diagram

As can be seen in Fig. 5, the flow field in the computational domain varies similarly under different pressure drops, and the speed will increase with pressure enhancement. The streamline can better characterize the motion pattern of the fluid. Because the cross-section in the entrance of the vacuum cleaner suddenly decreases, the fluid gathers here and presents a congestion phenomenon, which can be explained by the law of mass conservation. The reduction of the cross-section increases the turbulent kinetic energy of the fluid, therefore, a small range of eddies can be seen near the sides of the wall in vacuum cleaner.

The motion pattern of discrete iron filings is analyzed below, Fig. 6 shows the movement pattern and velocity distribution of iron filings when the iron filings fell 6s in the natural state shown as Fig. 6(a) and when the pressure drop is 100Pa, the time is t=2s, t=4s and t=6s, respectively, shown as Figs. 6(b)-(d).
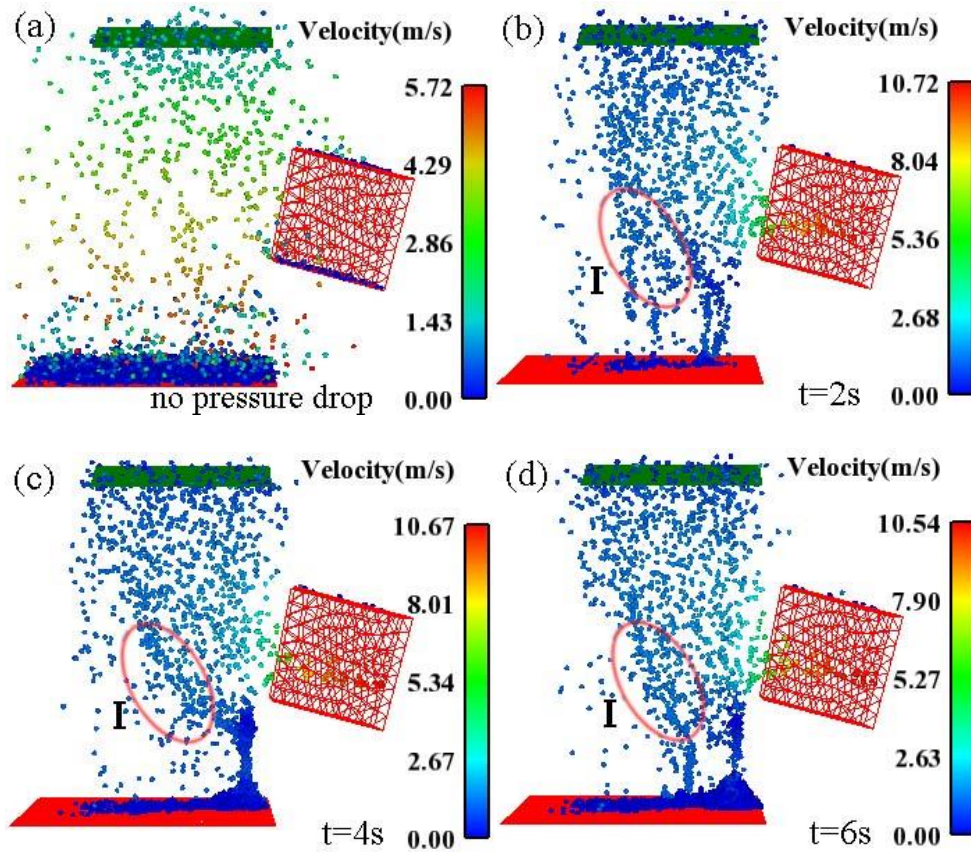
Fig. 6 The movement pattern and velocity distribution of iron filings under the inclination of 75°

Fig. 6(a) shows the movement pattern of iron filings when they peeled off the surface of the steel and fell 6s in the natural state, in which the initial velocity is defined as a random distribution of 0~2m/s in different directions and is generated at a rate of 1200 per second. The distribution of iron filings is wide and scattered and the maximum speed can reach 5.72m/s under the influence of gravity and coupling force. In the Figs. (b)-(c) and (d), with the increase of time, the iron filings gradually converge to the vacuum cleaner under the influence of coupling force, as shown in region **I**. And the iron filings near the vacuum cleaner are constantly sucked away under the negative pressure to provide space for the movement of the distant iron filings. It can be seen from the variation of maximum speed at each time that the maximum kinetic energy of iron filings decreases to some extent as more and more iron filings move toward the vacuum cleaner driven by the coupling force, which is manifested in the gradual reduction of velocity.

Fig. 7 shows the variation of the maximum coupling force and kinetic energy at the inlet of the vacuum cleaner with time at 75° inclination and 100Pa pressure drop. The maximum value of coupling force and kinetic energy has similar trend, which is mainly manifested in the increasing stage before 1s and the subsequent stable stage. There is a slight downward trend within the fluctuation range of 2~6s, mainly because the increasing number of iron filings consumes some turbulent kinetic energy over time, which is consistent with the analysis results in Fig. 6.
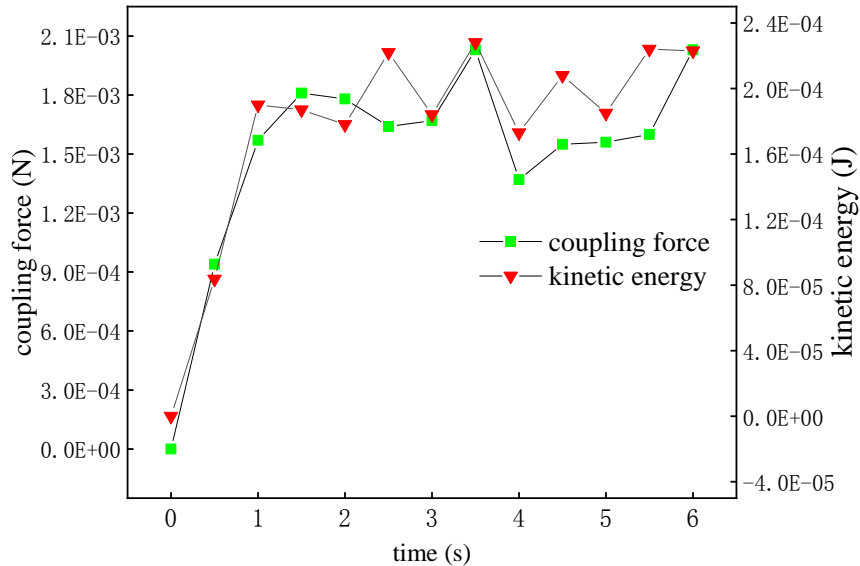
Fig. 7 Curves of coupling force and kinetic energy with time

4. Optimal calculation

4.1 Calculation preparation

In this part, two-fluid model is used to optimize the inlet angle of vacuum cleaner under the optimal results obtained by coupling CFD and DEM, and the calculation sketch is shown in Fig. 8. Ensure that the inlet area remains unchanged, the inlet angle $\theta =45° \sim 105°$ and the pressure drop $\Delta P =60pa \sim 120pa$ are taken as the free variables of the mass flow rate function at the outlet of the iron filings vacuum cleaner.

Add the basic attributes of iron filings $\rho = 7850 kg/m^3$, $d = 0.0005m$, the Eulerian two-fluid model was used to optimize the mass flow rate. In order to unify the mass of iron filings with the CFD-DEM coupling method, the volume fraction of iron filings phase was set to 0.05%, and the same time was calculated for 6s. The method of optimal space-filling design (OSF) was adopted, which can creates optimal space filling design of experiments plans according to the specified criteria and is able to distribute the design parameters equally throughout the design space with the objective of gaining the maximum insight into the design with the fewest number of points. And the Non-Parametric Regression was selected as the meta-model of response surface type, which provides improved response quality and is initialized with one of the available DOE types for predictably high nonlinear behavior of the outputs with respect to the inputs.

4.2 Results and discussion

The optimization calculation method can not only shorten the period of experiment or simulation, but also solve different objective functions according to the change of constraint conditions, which is favored by researchers. The results of the optimization calculation of 20 samples are shown in Table 4.
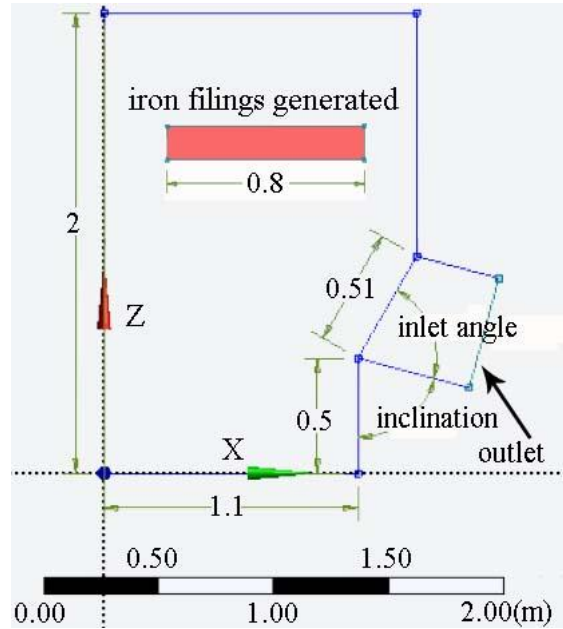
Fig. 8 Simulation sketch with two-fluid model

Table 4 Optimal results of 20 samples

|	Inlet angle(°)	Pressure drop(Pa)	Iron filings mass flow(Kg/s)
1	73.5	106.5	0.00868
2	52.5	109.5	0.03407
3	94.5	67.5	0.00086
4	67.5	82.5	0.01205
5	64.5	118.5	0.00493
6	61.5	100.5	0.02041
7	82.5	115.5	0.00277
8	97.5	112.5	0.00041
9	58.5	64.5	0.01077
10	46.5	94.5	0.03391
11	100.5	79.5	0.00093
12	76.5	91.5	0.00786
13	55.5	85.5	0.01965
14	85.5	76.5	0.00055
15	103.5	97.5	0.000001
16	49.5	73.5	0.02186
17	88.5	103.5	0.00062
18	79.5	61.5	0.00322
19	91.5	88.5	0.000275
20	70.5	70.5	0.01390
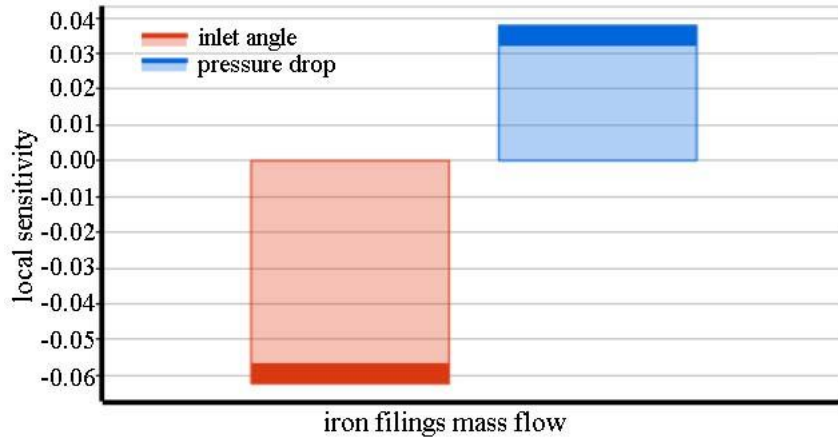
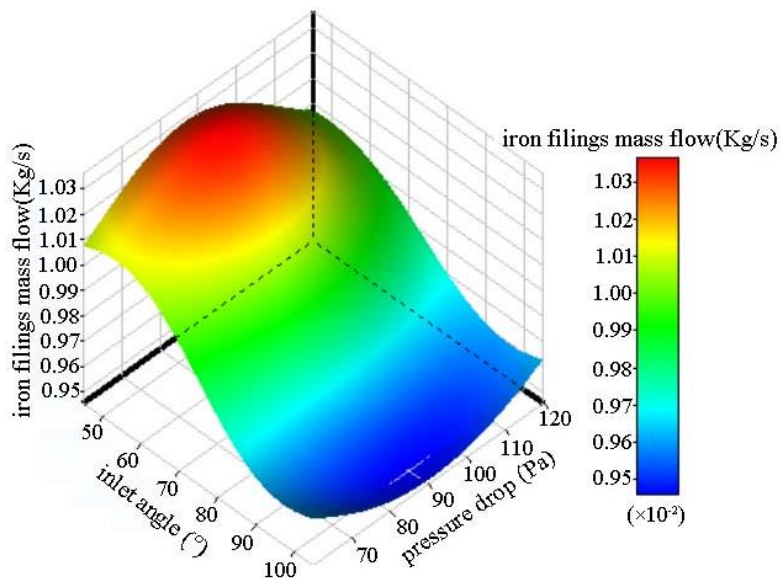Fig. 9 Sensitivity distribution of free variables

Fig. 10 Response surface of optimal results

The objective function of optimal calculation is the mass flow rate of iron filings, the value of which can indirectly reflect the iron filings collection efficiency. It can be seen from the table that the mass flow rate in the second group is the largest, that is to say, when the pressure drops is 109.5Pa and the inlet angle is 52.5°, the mass flow rate of iron filings 0.03407Kg/s is the maximum value of 20 samples of which the average value is 0.989×10^{-2}Kg/s.

Fig. 9 displays the distribution of the sensitivity of the free variable to the objective function, i.e. the degree of influence on the mass flow rate when the variables change. The red part in the figure represents the sensitivity of the inlet angle to the objective function, the value is about -0.062, indicating that the mass flow rate of the iron filings will decrease with the increase of the inlet angle. The blue part represents the sensitivity of the pressure drop to the objective function,
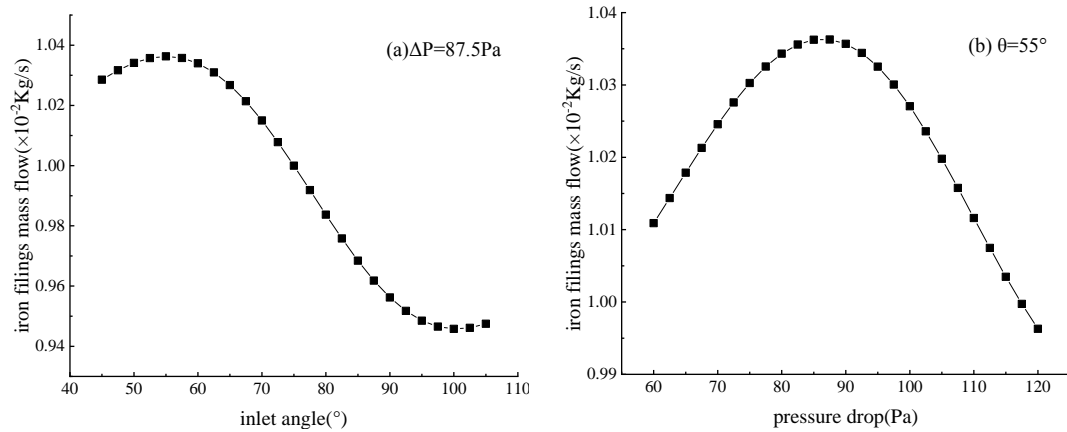
Fig. 11 Curve of iron filings mass flow rate with the single factor

and its value is about 0.038, which indicates that the mass flow rate is positively correlated with the pressure drop. From the absolute value of the sensitivity of the two, it can be seen that the value of the mass flow rate depends more on the inlet angle.

Fig. 10 shows a continuous response surface fitted by Non Parametric Regression method according to the results of the above 20 samples. The fitting method is based on the average of sample values, and the influence of eigenvalues on the results can be considered. The statistical analysis of the data on the response surface shows that the large value of the mass flow rate (greater than 1.02×10^{-2} Kg/s) is distributed in the area of the inlet angle $45° \sim 65°$ and the pressure drop 70Pa $\sim$ 100Pa, in which the corresponding pressure drop and the inlet angle of the largest mass flow rate are 87.5Pa and 55°, respectively. The influence of single factor on the mass flow rate of iron filings is simply analyzed by using the control variable method respectively, as shown in Fig. 11.

It can be seen from Fig. 11 that when the pressure drop ΔP=87.5Pa remains unchanged, the mass flow rate of iron filings increases slowly with the inlet angle, then decreases gradually to a constant. And the mass flow rate increases first and then decreases with the pressure drop when the inlet angle remains constant at 55°.

5. Conclusions

In this study, the CFD-DEM coupling model and two-fluid model are used to optimize the iron filings collection efficiency of vacuum cleaner used in steel processing plants, and the following conclusions are obtained.

• For the randomly distributed iron filings generated in steel processing, the vacuum cleaner can be laid at the inclination of 75° or 90° to the vertical direction. And when the pressure drop is between 40Pa $\sim$ 100Pa, the collection efficiency at 75° is greater than that other inclinations. As for the inclination of 90°, only when the pressure drop exceeds 120Pa, the collection efficiency can reach the maximum value.

• Through the analysis of the flow field, the coupling force and kinetic energy at the inlet of the vacuum cleaner and the distribution of iron filings at different time, we know that during the

working of the vacuum cleaner, the iron filings will gradually move towards the vacuum cleaner under the influence of coupling force, resulting in aggregation phenomenon. At the same time, the increasing number of iron filings consumed a certain turbulent kinetic energy, which is mainly manifested in the slight reduction of the iron filings speed.

• The inlet angle and pressure drop corresponding to the optimal solution of 20 samples generated by OSF method are 52.5° and 109.5Pa respectively based on the two-fluid model. Sensitivity analysis shows that the mass flow rate of iron filings depends more on the change of the inlet angle. The surface fitting result of 20 sample values by NPR method shows that the larger mass flow rate of iron filings is distributed in the region of the inlet angle with 45° ~ 65° and the pressure drop with 70 Pa ~100 Pa.

Acknowledgement

References

Almohammed, N., Alobaid, F., Breuer, M. and Epple, B. (2014), "A comparative study on the influence of the gas flow rate on the hydrodynamics of a gas-solid spouted fluidized bed using Euler–Euler and Euler-Lagrange/DEM models", *Powder Technol.*, **264**, 343-364. https://doi.org/10.1016/j.powtec.2014.05.024.

Alobaid, F. and Epple, B. (2013), "Improvement, validation and application of CFD/DEM model to dense gas-solid flow in a fluidized bed", *Particuology*, **11**(5), 514-526. https://doi.org/10.1016/j.partic.2012.05.008.

Chu, K.W., Wang, B., Yu, A.B. and Vince, A. (2009), "CFD-DEM modelling of multiphase flow in dense medium cyclones", *Powder Technol.*, **193**(3), 235-247. https://doi.org/10.1016/j.powtec.2009.03.015

Crowe, C., Sommerfeld, M. and Tsuji, Y. (1998), *Multiphase Flows with Droplets and Particles*, CRC Press, Boca Raton, Florida, USA.

Cundall, P.A. and Strack, O.D.L. (1979), "A discrete numerical model for granular assemblies", *Géotechnique*, **29**(1), 47-65. https://doi.org/10.1680/geot.1979.29.1.47.

DesignXplorer ANSYS (2013), *Workbench DesignXplorer Theory User's Manual*, Release 15.0.

Dhurandhar, R., Sarkar, J.P. and Das, B. (2019). "Elucidation of hydrodynamics and heat transfer characteristic of converging and equivalent uniform riser for dilute phase gas–solid flow", *Chem. Eng. Res. Design*, **151**, 120-130. https://doi.org/10.1016/j.cherd.2019.09.002.

Du, W., Bao, X., Xu, J. and Wei, W. (2006), "Computational fluid dynamics (CFD) modeling of spouted bed: assessment of drag coefficient correlations", *Chemical Eng. Sci.*, **61**(5), 1401–1420. https://doi.org/10.1016/j.ces.2005.08.013.

Du, W., Bao, X., Xu, J. and Wei, W. (2006), "Computational fluid dynamics (CFD) modeling of spouted bed: influence of frictional stress, maximum packing limit and coefficient of restitution of particles", *Chem. Eng. Sci.*, **61**(14), 4558–4570. https://doi.org/10.1016/j.ces.2006.02.028.

Feng, Y.T. and Owen, D.R.J. (2014), "Discrete element modelling of large scale particle systems-I: exact scaling laws", *Comput. Particle Mech.*, **1**(2), 159-168. https://doi.org/10.1007/s40571-014-0010-y

Gidaspow, D. (1994), *Multiphase Flow and Fluidization: Continuum and Kinetic Theory Description*, Academic Press, San Diego, USA.

Hobbs, A. (2009), "Simulation of an aggregate dryer using coupled CFD and DEM methods", *J. Comput. Fluid Dynam.*, **23**(2), 199-207. https://doi.org/10.1080/10618560802680971

Hoomans, B.P.B., Kuipers, J.A.M., Briels, W.J. and Van Swaaij, W.P.M. (1996), "Discrete particle

simulation of bubble and slug formation in a two-dimensional gas-fluidised bed: A hard-sphere approach", *Chem. Eng. Sci.*, **51**(1), 99-118. https://doi.org/10.1016/0009-2509(95)00271-5.

Liu, H.X., Liu, M., Jiao, L., Zhao, L., Luo, J., Xu, D. and Guo, Y. (2018), "Numerical simulation of gas-solid two-phase flow in electrostatic precipitator of 1000MW unit", *Chinese J. Environ. Eng.*, **12**(7), 2029-2038. (In Chinese).

Ma, J., Wang, C.B., Ren, Y.J. and Hu, J. (2019), "Numerical Simulation and Optimization Design of Gas-solid Two-phase Flow in Flexible Membrane High Temperature Dust Filter", *J. North China Electric Power University*, **46**(1), 95-102. (In Chinese)

Mathiesen, V., Solberg, T. and Hjertager, B.H. (2000), "Predictions of gas/particle flow with an Eulerian model including a realistic particle size distribution", *Powder Technol.*, **112**(1-2), 34-45. https://doi.org/10.1016/S0032-5910 (99)00303-4.

Miao, Z., Kuang, S.B., Zughbi, H. and Yu, A.B. (2019), "CFD simulation of dilute-phase pneumatic conveying of powders", *Powder Technol.*, **349**, 70-83. https://doi.org/10.1016/j.powtec.2019.03.031

Patro, P. and Dash, S.K., (2014), "Numerical Simulation for Hydrodynamic Analysis and Pressure Drop Prediction in Horizontal Gas-Solid Flows", *Particulate Sci. Technol.*, **32**(1), 94-103. https://doi.org/10.1080/02726351.2013.829543.

Patro, P. and Dash, S.K., (2014), "Two-fluid modeling of turbulent particle–gas suspensions in vertical pipes", *Powder Technol.*, **264**, 320-331. https://doi.org/10.1016/j.powtec.2014.05.048.

Ray, M., Chowdhury, F., Sowinski, A., Mehrani, P. and Passalacqua, A. (2019), "An Euler-Euler model for mono-dispersed gas-particle flows incorporating electrostatic charging due to particle-wall and particle-particle collisions", *Chem. Eng. Sci.*, **197**, 327-344. https://doi.org/10.1016/j.ces.2018.12.028.

Xu, B.H. and Yu, A.B. (1997), "Numerical simulation of the gas-solid flow in a fluidized bed by combining discrete particle method with computational fluid dynamics", *Chem. Eng. Sci.*, **52**(16), 2785-2809. https://doi.org/10.1016/S0009-2509(97)00081-X.

Xu, S.L., Sun, R., Cai, Y. Q. and Sun, H.L. (2018), "Study of sedimentation of non-cohesive particles via CFD–DEM simulations", *Granular Matter*, **20**(1), 4. https://doi.org/10.1007/s10035-017-0769-7.

Yu, A.B. and Xu, B.H. (2003), "Particle-scale modelling of gas-solid flow in fluidization", *J. Chem. Technol. Biotechnol.,* **78**(2-3), 111-121. https://doi.org/10.1002/jctb.788.

Zhang, H., Li, T., Huang, Z., Kuang, S. and Yu, A. (2018), "Investigation on vertical plug formation of coarse particles in a non-mechanical feeder by CFD-DEM coupling method", *Powder Technol.*, **332**, 79-89. https://doi.org/10.1016/j.powtec.2018.03.055.

Zhou, Z.Y., Kuang, S.B., Chu, K.W. and Yu, A.B. (2010), "Discrete particle simulation of particle-fluid flow: model formulations and their applicability", *J. Fluid Mech.*, **661**, 482-510. https://doi.org/10.1017/S002211201000306X.

Zhu, H.P., Zhou, Z.Y., Yang, R.Y. and Yu, A.B. (2007), "Discrete particle simulation of particulate systems: theoretical developments", *Chem. Eng. Sci.*, **62**(13), 3378-3396. https://doi.org/10.1016/j.ces.2006.12.089.

TK